

Three-body Casimir effects and non-monotonic forces

P. Rodriguez-Lopez,¹ S. J. Rahi,² and T. Emig^{3,4}

¹*Departamento de Fisica Aplicada I, Universidad Complutense, 28040 Madrid, Spain*

²*Massachusetts Institute of Technology, Department of Physics,
77 Massachusetts Avenue, Cambridge, MA 02139, USA*

³*Institut für Theoretische Physik, Universität zu Köln, Zùlpicher Strasse 77, 50937 Köln, Germany*

⁴*Laboratoire de Physique Théorique et Modèles Statistiques,
CNRS UMR 8626, Université Paris-Sud, 91405 Orsay, France*

(Dated: November 8, 2021)

Casimir interactions are not pair-wise additive. This property leads to collective effects that we study for a pair of objects near a conducting wall. We employ a scattering approach to compute the interaction in terms of fluctuating multipoles. The wall can lead to a non-monotonic force between the objects. For two atoms with anisotropic electric and magnetic dipole polarizabilities we demonstrate that this non-monotonic effect results from a competition between two- and three body interactions. By including higher order multipoles we obtain the force between two macroscopic metallic spheres for a wide range of sphere separations and distances to the wall.

PACS numbers: 42.25.Fx, 03.70.+k, 12.20.-m.

A hallmark property of dispersion forces is their non-additivity which clearly distinguishes them from electromagnetic forces between charged particles [1]. Work on the interactions between multiple objects is limited mostly to atoms or small particles which are described well in dipole approximation [2]. This approximation cannot be used for macroscopic objects at separations that are comparable to their size since higher order multipole fluctuations have to be included [3, 4]. In such situations, also other common “additive” methods such as proximity or two-body-interaction approximations fail. Three-body effects for macroscopic bodies have been studied in quasi two-dimensional (2D) geometries that are composed of parallel perfect metal cylinders of quadratic [5] or circular [6, 7] cross section and parallel sidewalls. For this setup non-monotonic forces have been found and interpreted as resulting from a competition between electric and magnetic polarizations which are decoupled for quasi 2D geometries of perfect metal structures. In this Letter we investigate collective 3-body effects between *compact* objects, including anisotropic polarizabilities, and a wall in three dimensions using a recently developed scattering approach [4, 8]. This allows us to observe the influence of polarization coupling and anisotropy on non-monotonic effects.

We consider the retarded Casimir interaction between a pair of atoms with anisotropic electric and magnetic polarizabilities near a conducting wall, see Fig. 1. We identify a competition between 2- and 3-body effects and prove that this leads to a non-monotonic dependence of the force between the atoms on the wall separation H for *each* of the four possible polarizations of fluctuations (electric/magnetic and parallel/perpendicular to the wall) *separately*. For isotropic polarizabilities we find that only the force component due to electric fluctuations is non-monotonic in H . This findings suggest the possi-

bility to engineer the monotonicity properties of the force by suitable tailoring of the polarization tensors via the shape and material composition of macroscopic particles.

For atoms, magnetic effects are almost always rather small in the retarded limit. Contrary to this, for conducting macroscopic objects contributions from electric and magnetic multipole fluctuations are comparable. To study the effect of higher-order multipoles, we consider also two perfect metal spheres near a wall, see Fig. 1. Based on consistent analytical results for large separations and numerical computations at smaller distances we find a non-monotonic dependence of the force between the spheres on H . Unlike for atoms, this effect is occurs at sufficiently large sphere separations only.

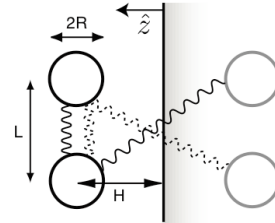


FIG. 1: Geometry of the two-sphere/atom and sidewall system. Shown are also the mirror images (grey) and two- and three-body contributions (solid and dashed curly lines, respectively).

As derived by Refs. [4, 8], the Casimir energy of two bodies in the presence of a perfectly conducting sidewall can be obtained within a scattering approach by employing the method of images that introduces fluctuating currents on the mirror bodies. The Casimir energy of the original system is then given by the energy of the original and the image objects and it can be expressed as an integral over imaginary wave number,

$$\mathcal{E} = \frac{\hbar c}{2\pi} \int_0^\infty d\kappa \ln \det(\mathbb{M} \mathbb{M}_\infty^{-1}) \quad (1)$$

with the matrix

$$\mathbb{M} = \begin{pmatrix} \mathbb{T}^{-1} + \mathbb{U}^{I,11} & \mathbb{U}^{12} + \mathbb{U}^{I,12} \\ \mathbb{U}^{21} + \mathbb{U}^{I,21} & \mathbb{T}^{-1} + \mathbb{U}^{I,22} \end{pmatrix}, \quad (2)$$

which is given by the T-matrix \mathbb{T} that relates the incoming and scattered electromagnetic (EM) fields for each body, and by the U-matrices $\mathbb{U}^{\alpha\beta}$, $\mathbb{U}^{I,\alpha\beta}$ that describe the interaction between the multipoles of object α and object β and between the multipoles of object α and the image of object β , respectively. The T-matrix depends only on properties of the bodies such as polarizability or size and shape. The U-matrices depend only on the distance vector between the objects and decay exponentially with distance and wave number κ . The matrix \mathbb{M}_∞ accounts for the subtraction of the object's self-energies and hence follows from \mathbb{M} by taking the limit of infinite separations, i.e., by setting all U-matrices to zero. For a multipole expansion the matrix elements are computed in a vector spherical basis for the EM field with partial wave

numbers $l \geq 1$, $m = -l, \dots, l$. (Details of this expansion and the U-matrix elements can be found in Ref. [8].)

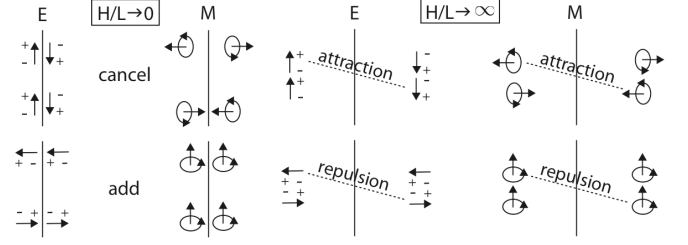


FIG. 2: Typical orientations of electric (E) and magnetic (M) dipoles and image dipoles for $H/L \rightarrow 0$ and $H/L \rightarrow \infty$.

In the following we study the force $F = -\partial\mathcal{E}/\partial L$ between the two objects at separation L and hence eliminate the contributions to the energy that depend only on the sidewall separation H , see Fig. 1. We expand the determinant of Eq. (1) as

$$\det(\mathbb{M}\mathbb{M}_\infty^{-1}) = \det(1 + \mathbb{T}\mathbb{U}^I) \det(1 + \mathbb{T}\mathbb{U}^I) \det[1 - (1 + \mathbb{T}\mathbb{U}^I)^{-1}\mathbb{T}(\mathbb{U}^{21} + \mathbb{U}^{I,21})(1 + \mathbb{T}\mathbb{U}^I)^{-1}\mathbb{T}(\mathbb{U}^{12} + \mathbb{U}^{I,12})]. \quad (3)$$

The first two determinants on the r.h.s. yield together twice the interaction energy between a single object and the sidewall since $\mathbb{U}^I \equiv \mathbb{U}^{I,11} = \mathbb{U}^{I,22}$ describes the multipole coupling between one object and its image and hence depends only on H . Hence, we consider only the energy \mathcal{E}_{oo} that corresponds to the last determinant of Eq. (3) and provides the potential energy of the two objects in the presence of the sidewall so that $F = -\partial\mathcal{E}_{\text{oo}}/\partial L$. In the absence of the sidewall, $H \rightarrow \infty$, the matrices $\mathbb{U}^{I,\alpha\beta}$ all vanish and \mathcal{E}_{oo} simplifies to the energy between two spheres [4]. For an interpretation in terms of multiple scatterings, it is instructive to use the relation $\ln \det = \text{Tr} \ln$ and to expand the logarithm which yields

$$\mathcal{E}_{\text{oo}} = -\frac{\hbar c}{2\pi} \int_0^\infty d\kappa \sum_{p=1}^\infty \frac{1}{p} \text{Tr} \left[\sum_{n=0}^\infty (-1)^n (\mathbb{T}\mathbb{U}^I)^n \mathbb{T}(\mathbb{U}^{21} + \mathbb{U}^{I,21}) \sum_{n'=0}^\infty (-1)^{n'} (\mathbb{T}\mathbb{U}^I)^{n'} \mathbb{T}(\mathbb{U}^{12} + \mathbb{U}^{I,12}) \right]^p, \quad (4)$$

where we have written the inverse matrices of Eq. (3) as series. The trace acts on an alternating product of T- and U-matrices which describe scattering and free propagation of EM fluctuations, respectively. Multiple scatterings between an object and its image ($\mathbb{T}\mathbb{U}^I$) are followed by a propagation to the other object-image pair, either to the object (\mathbb{U}^{21}) or its image ($\mathbb{U}^{I,21}$), between which again multiple scatterings occur before the fluctuations are scattered back to the initial object or its image (\mathbb{U}^{12} or $\mathbb{U}^{I,12}$) and the process repeats. This expansion is useful for small objects or large separations.

As the first application, we consider the case of two identical, ground state atoms near a wall, see Fig. 1. The separation between the atoms is L and they have equal distance H from the wall. In dipole approximation, the retarded limit of the interaction is described by the static electric (α_z , α_\parallel) and magnetic (β_z , β_\parallel) dipole polarizabilities of the atoms which can be different perpendicular (z) and parallel (\parallel) to the wall. The T-matrix of the atoms is diagonal and has finite elements only for the dipole channel (partial waves with $l = 1$), given by $T_{10}^E = \frac{2}{3}\alpha_z\kappa^3$,

$T_{1m}^E = \frac{2}{3}\alpha_\parallel\kappa^3$ for electric and $T_{10}^M = \frac{2}{3}\beta_z\kappa^3$, $T_{1m}^M = \frac{2}{3}\beta_\parallel\kappa^3$ for magnetic polarization with $m = \pm 1$. For atoms, the polarizability is much smaller than L^3 , and hence it is sufficient to compute the interaction to second order in the polarizabilities. This amounts to consider only the terms with $p = 1$, $n = n' = 0$ of Eq. (4). The resulting energy \mathcal{E}_{oo} is then compared to the well-known Casimir-Polder (CP) interaction between two atoms (without the wall)

$$\mathcal{E}_{2,\parallel}(L) = -\frac{\hbar c}{8\pi L^7} [33\alpha_\parallel^2 + 13\alpha_z^2 - 14\alpha_\parallel\beta_z + (\alpha \leftrightarrow \beta)] \quad (5)$$

which corresponds to the sequence $\mathbb{T}\mathbb{U}^{21}\mathbb{T}\mathbb{U}^{12}$ in Eq. (4). The total interaction energy is

$$\mathcal{E}_{\text{oo}}(L, H) = \mathcal{E}_{2,\parallel}(L) + \mathcal{E}_{2,\setminus}(D, L) + \mathcal{E}_3(D, L) \quad (6)$$

with $D = \sqrt{L^2 + 4H^2}$. The 2-body energy $\mathcal{E}_{2,\setminus}(D, L)$ comes from the sequence $\mathbb{T}\mathbb{U}^{I,21}\mathbb{T}\mathbb{U}^{I,12}$ in Eq. (4) and hence is the usual CP interaction between one atom and

the image of the other atom (see Fig. 1). The change in the relative orientation of the atoms with $\ell = L/D$ leads

$$\mathcal{E}_{2,\setminus}(D, L) = -\frac{\hbar c}{8\pi D^7} \left[26\alpha_{\parallel}^2 + 20\alpha_z^2 - 14\ell^2(4\alpha_{\parallel}^2 - 9\alpha_{\parallel}\alpha_z + 5\alpha_z^2) + 63\ell^4(\alpha_{\parallel} - \alpha_z)^2 - 14(\alpha_{\parallel}\beta_{\parallel}(1-\ell^2) + \ell^2\alpha_{\parallel}\beta_z) + (\alpha \leftrightarrow \beta) \right]. \quad (7)$$

The 3-body energy $\mathcal{E}_3(D, L)$ corresponds to the sequences $\text{TU}^{21}\text{TU}^{I,12}$, $\text{TU}^{I,21}\text{TU}^{12}$ in Eq. (4) and hence describes the collective interaction between the two atoms and one image atom. It is given by

$$\mathcal{E}_3(D, L) = \frac{4\hbar c}{\pi} \frac{1}{L^3 D^4 (\ell + 1)^5} \left[(3\ell^6 + 15\ell^5 + 28\ell^4 + 20\ell^3 + 6\ell^2 - 5\ell - 1) (\alpha_{\parallel}^2 - \beta_{\parallel}^2) - (3\ell^6 + 15\ell^5 + 24\ell^4 - 10\ell^2 - 5\ell - 1) (\alpha_z^2 - \beta_z^2) + 4(\ell^4 + 5\ell^3 + \ell^2) (\alpha_z\beta_{\parallel} - \alpha_{\parallel}\beta_z) \right]. \quad (8)$$

For isotropic electric polarizable atoms this result agrees with that of Ref. [2]. It is instructive to consider the two limits $H \ll L$ and $H \gg L$. For $H \ll L$ one has $D \rightarrow L$ and the 2-body potentials are identical, $\mathcal{E}_{2,\setminus}(L, L) = \mathcal{E}_{2,|}(L)$. The 3-body energy becomes

$$\mathcal{E}_3(L, L) = -\frac{\hbar c}{4\pi L^7} \left[-33\alpha_{\parallel}^2 + 13\alpha_z^2 + 14\alpha_{\parallel}\beta_z - (\alpha \leftrightarrow \beta) \right]. \quad (9)$$

The total energy \mathcal{E}_{oo} is now twice the energy of Eq. (5) plus the energy of Eq. (9) and hence \mathcal{E}_{oo} becomes the CP potential of Eq. (5) with the replacements $\alpha_z \rightarrow 2\alpha_z$, $\alpha_{\parallel} \rightarrow 0$, $\beta_z \rightarrow 0$, $\beta_{\parallel} \rightarrow 2\beta_{\parallel}$, i.e., the 2-body and 3-body contributions add constructively or destructively, depending on the relative orientation of a dipole and its image which together form a dipole of zero or twice the original strength (see Fig. 2). For $H \gg L$ the leading correction to the CP potential of Eq. (5) comes from the 3-body energy which in this limit becomes to order H^{-6}

$$\mathcal{E}_3(H, L) = \frac{\hbar c}{\pi} \left[\frac{\alpha_z^2 - \alpha_{\parallel}^2}{4L^3 H^4} + \frac{9\alpha_{\parallel}^2 - \alpha_z^2 - 2\alpha_{\parallel}\beta_z}{8LH^6} - (\alpha \leftrightarrow \beta) \right]. \quad (10)$$

The signs of the polarizabilities in the leading term $\sim H^{-4}$ can be understood from the relative orientation of the dipole of one atom and the image dipole of the other atom, see Fig. 2. If these two electric (magnetic) dipoles are almost perpendicular to their distance vector they contribute attractively (repulsively) to the potential between the two original atoms. If these electric (magnetic) dipoles are almost parallel to their distance vector they yield a repulsive (attractive) contribution. For isotropic polarizabilities the leading term of Eq. (10) vanishes and the electric (magnetic) part $\sim H^{-6}$ of the 3-body energy is always repulsive (attractive).

The above results determine the variation of the force between the two particles with H . If the two particles have only either α_z or β_{\parallel} polarizability, their attractive force is *reduced* when they approach the wall from large H due to the repulsive 3-body energy. At close proximity to the wall the fluctuations of the dipole and its image add up to yield a force between the particles that is *enhanced* by a factor of 4 compared to the force for $H \rightarrow \infty$.

to the modified CP potential

Equivalent arguments show that the force between particles with either α_{\parallel} or β_z polarizability is *enhanced* at large H and *reduced* to zero for $H \rightarrow 0$. This proves that the force between particles which both have either of the four polarizabilities is always non-monotonic. The situation can be different if more than one polarizability is finite, especially for isotropic particles. In the latter case all contributions (electric, magnetic, mixed) are enhanced for $H \rightarrow 0$ and only the electric term is reduced at large H so that only the electric part gives a non-monotonic force. In general, the monotonicity property depends on the relative strength and anisotropy of the electric and magnetic polarizabilities.

As the second application we study two macroscopic perfect metallic spheres of radius R for the same geometry as in the case of atoms where the lengths L and H are measured now from the centers of the spheres, see Fig. 1. The T-matrix is diagonal and the elements $T_{lm}^M = (-1)^l \frac{\pi}{2} I_{l+1/2}(\kappa R) / K_{l+1/2}(\kappa R)$, $T_{lm}^E = (-1)^l \frac{\pi}{2} [I_{l+1/2}(\kappa R) + 2\kappa R I'_{l+1/2}(\kappa R)] / [K_{l+1/2}(\kappa R) + 2\kappa R K'_{l+1/2}(\kappa R)]$ are given in terms of the Bessel functions I_{ν} , K_{ν} . First, we expand the energy in powers of R by using Eq. (4) which implies that we expand the T-matrices for small frequencies but use the exact expressions for the U-matrices. For $R \ll L, H$ and arbitrary H/L the result for the force can be written as

$$F = \frac{\hbar c}{\pi R^2} \sum_{j=6}^{\infty} f_j(H/L) \left(\frac{R}{L} \right)^{j+2}. \quad (11)$$

The f_j can be computed exactly. We have obtained them up to $j = 11$ and the first three are (with $s \equiv \sqrt{1 + 4h^2}$)

$$f_6(h) = -\frac{1}{16h^8} \left[s^{-9}(18 + 312h^2 + 2052h^4 + 6048h^6 + 5719h^8) + 18 - 12h^2 + 1001h^8 \right], \quad f_7(h) = 0, \quad (12)$$

$$f_8(h) = -\frac{1}{160h^{12}} \left[s^{-11}(6210 + 140554h^2 + 1315364h^4 + 6500242h^6 + 17830560h^8 + 25611168h^{10} + 15000675h^{12}) - 6210 - 3934h^2 + 764h^4 - 78h^6 + 71523h^{12} \right]. \quad (13)$$

The coefficient f_7 of R^7 vanishes since a multipole of order l contributes to the T-matrix at order R^{2l+1} so that beyond the two-dipole term $\sim R^6$ the next term comes from a dipole ($l = 1$) and a quadrupole ($l = 2$), yielding f_8 . For $H \gg L$ one has $f_6(h) = -1001/16 + 3/(4h^6) + \mathcal{O}(h^{-8})$, $f_8(h) = -71523/160 + 39/(80h^6) + \mathcal{O}(h^{-8})$ so that the wall induces weak repulsive corrections. For $H \ll L$, $f_6(h) = -791/8 + 6741h^2/8 + \mathcal{O}(h^4)$, $f_8(h) = -60939/80 + 582879h^2/80 + \mathcal{O}(h^4)$ so that the force amplitude decreases when the spheres are moved a small distance away from the wall. This proves the existence of a minimum in the force amplitude as function of H/R for fixed, sufficiently small R/L . We note that all $f_j(h)$ are finite for $h \rightarrow \infty$ but some diverge for $h \rightarrow 0$, e.g., $f_9 \sim f_{11} \sim h^{-3}$, making them important for small H .

To obtain the interaction at smaller separations or larger radius, we have computed the energy \mathcal{E}_{oo} and force $F = -\partial\mathcal{E}_{\text{oo}}/\partial L$ between the spheres numerically. For the energy, we have computed the last determinant of Eq. (3) and the integral over κ of Eq. (1) numerically. The force is obtained by polynomial interpolation of the data for the energy. The matrices are truncated at a sufficiently large number of partial waves (with a maximum truncation order $l_{\text{max}} = 17$ for the smallest separation) so that the relative accuracy of the values for \mathcal{E}_{oo} is $\approx 10^{-3}$. The data for $H/R = 1$ are obtained by extrapolation in l_{max} . The results are shown in Figs. 3, 4. In order to show the effect of the wall, the figures display the energy and force normalized to the results for two spheres without a wall. Fig. 3 shows the energy and force as function of the (inverse) separation between the spheres for different fixed wall distances. Energy and force show an increasing relative enhancement due to the wall with increasing L , with the maximal enhancement for small H . For sufficiently large H/R , the energy and force ratios are non-monotonic in L and can be slightly smaller than without the wall. Fig. 4 shows the force as function of the wall distance for fixed L . When the spheres approach the wall, the force first decreases slightly if $R/L \lesssim 0.3$ and then increases strongly under a further reduction of H . For $R/L \gtrsim 0.3$ the force monotonically increases towards the wall. This agrees with the prediction of the large distance expansion. The expansion of Eq. (11) with $j = 10$ terms is also shown in Fig. 4 for $R/L \leq 0.2$. Its validity is limited to large L/R and not too small H/R ; it fails completely for $R/L > 0.2$ and hence is not shown in this range.

Our results for atoms are potentially relevant to the interaction between trapped Bose-Einstein condensates and a surface [9] at close surface separations. The results for macroscopic spheres could be important for the design of nano-mechanical devices where small components operate in close vicinity to metallic boundaries. Generally, the wall-induced enhancement of the interaction can make the experimental observation of Casimir forces between small particles more feasible. The reported dependence on the anisotropy of polarizabilities suggest in-

teresting effects for objects of non-spherical shape.

We acknowledge helpful discussions with N. Graham, R. L. Jaffe, and M. Kardar, and the hospitality of the Institute of Theoretical Physics, University of Cologne. This research was supported by projects MOSAICO, UCM/PR34/07-15859 and a PFU MEC grant (PR) and by DFG through grant EM70/3 (TE).

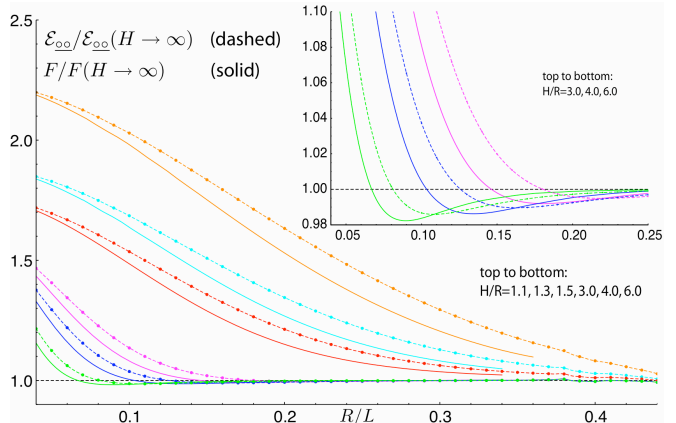


FIG. 3: Numerical results for the potential energy (dashed curves) and force (solid curves) between two spheres as function of R/L for different sidewall separations H/R . Both force and energy are normalized to their values in the absence of the sidewall. Inset: Magnification of behavior for small R/L .

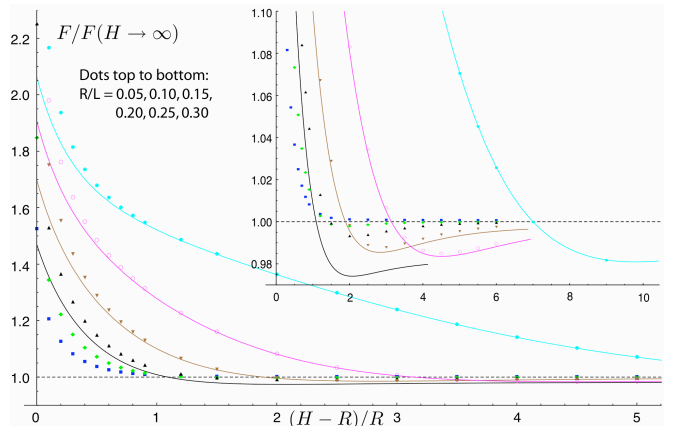


FIG. 4: Numerical results for the force (dots) between two spheres as function of the sidewall separation H/R for different sphere separations R/L . Shown are also the analytical results of Eq. (11), including terms up to $j = 10$ for $R/L \leq 0.2$ (solid curves). Inset: Magnification of the non-monotonicity.

- [1] V. A. Parsegian, *Van der Waals Forces* (Cambridge University Press, Cambridge, England, 2005).
- [2] E. A. Power and T. Thirunamachandran, *Phys. Rev. A* **25**, 2473 (1982).
- [3] G. Feinberg, *Phys. Rev. B* **9**, 2490 (1974).
- [4] T. Emig, N. Graham, R. L. Jaffe, and M. Kardar, *Phys. Rev. Lett.* **99**, 170403 (2007).
- [5] A. W. Rodriguez, M. Ibanescu, D. Iannuzzi, F. Capasso, J. D. Joannopoulos, and S. G. Johnson, *Phys. Rev. Lett.* **99**, 080401 (2007).

- [6] S. J. Rahi, A. W. Rodriguez, T. Emig, R. L. Jaffe, S. G. Johnson, and M. Kardar, Phys. Rev. A **77**, 030101 (2008).
- [7] S. J. Rahi, T. Emig, R. L. Jaffe, and M. Kardar, Phys. Rev. A **78**, 012104 (2008).
- [8] T. Emig, Journal of Statistical Mechanics: Theory and Experiment **4**, P04007 (2008).
- [9] D. M. Harber, J. M. Obrecht, J. M. McGuirk, and E. A. Cornell, Phys. Rev. A **72**, 033610 (2005).